Parton collisional effect on the conversion of geometry eccentricities into momentum anisotropies in relativistic heavy-ion collisions

Long Ma,[1,*] Guo-Liang Ma,[1,†] and Yu-Gang Ma[1,2,‡]
[1]*Key Laboratory of Nuclear Physics and Ion-beam Application (MOE), Institute of Modern Physics, Fudan University, Shanghai 200433, China*
[2]*Shanghai Institute of Applied Physics, Chinese Academy of Sciences, Shanghai 201800, China*

(Received 7 October 2020; accepted 22 December 2020; published 29 January 2021)

We explore parton collisional effects on the conversion of geometry eccentricities into azimuthal anisotropies in Pb + Pb collisions at $\sqrt{s_{NN}} = 5.02$ TeV using a multiphase transport model. The initial eccentricity ε_n ($n = 2, 3$) and flow harmonics v_n ($n = 2, 3$) are investigated as a function of the number of parton collisions ($N_{\rm coll}$) during the source evolution of partonic phase. It is found that partonic collisions leads to generate elliptic flow v_2 and triangular flow v_3 in Pb + Pb collisions. On the other hand, partonic collisions also result in an evolution of the eccentricity of geometry. The collisional effect on the flow conversion efficiency is therefore studied. We find that the partons with larger $N_{\rm coll}$ show a lower flow conversion efficiency, which reflects differential behaviors with respect to $N_{\rm coll}$. It provides an additional insight into the dynamics of the space-momentum transformation during the QGP evolution from a transport model point of view.

DOI: 10.1103/PhysRevC.103.014908

I. INTRODUCTION

In high-energy heavy-ion collisions, at the extreme conditions of high temperature and high baryon density, strongly interacting quark gluon plasma (QGP) is expected to be created. The pressure gradient of the initial compressed QGP leads to an anisotropic expansion and transfers initial-state spatial anisotropy to the final-state momentum azimuthal anisotropy, which can be measured through momentum information of the final charged hadrons [1–7]. Characterized by the flow coefficients v_n ($n = 2, 3, 4$), azimuthal anisotropies of the final-state particles are suggested to be sensitive to not only the early stage partonic dynamics but also properties of the source [8–12]. Experimentally, systematic studies have been performed for v_n in both large heavy-ion collision systems and small collision systems [13–21]. Sizable v_n observed in experiment indicates that the hot and dense QGP source is like a nearly perfect fluid.

Due to the fluidlike behavior observed for QGP, hydrodynamic models have been widely used to make predictions and are successful in describing flow harmonics at energies available at both the BNL Relativistic Heavy Ion Collider (RHIC) and the CERN Large Hadron Collider (LHC) [22–29]. Besides hydrodynamic models, a multiphase transport model (AMPT) is also employed in studies of anisotropic flow in high energy collisions. Including both partonic and hadronic interactions, a multiphase transport model can reasonably reproduce experimental flow measurements in both large and small collision systems [30–37].

In recent years, an escape mechanism was proposed, challenging the commonly believed hydrodynamical origin of the flow anisotropies [38,39]. It was found that, instead of collectivity from partonic interactions, anisotropic parton escape dominates the flow generation in the d + Au collision system as well as semicentral Au + Au collisions. Though parton escape makes a considerable contribution, it was also realized that partonic interaction is essential for generating v_n in strongly interacting systems, and v_n from partonic interaction becomes dominant in collision systems with large parton-parton interaction cross section. Extensive studies have been performed on the harmonic flow, dihadron correlation, and energy loss induced by partonic collisions [40–46].

Theoretically, final flow anisotropy is suggested to be strongly correlated with the initial geometric anisotropy in relativistic heavy-ion collisions [11,47–54]. It has been argued that the magnitude and trend of the partonic participant eccentricity ε_n ($n = 2, 3$) imply specifically testable predictions for the final flow harmonics [55–57]. For a deeper understanding of the transport, it is essential to investigate the parton collisional effect on the initial geometric anisotropy as well as the conversion from coordinate space to momentum space, which is expected to provide important information about the evolution dynamics of early stage.

In this paper, we present a systematic study of the partonic collision effect on the initial eccentricity and flow anisotropy in high energy Pb + Pb collisions at $\sqrt{s_{NN}} = 5.02$ TeV, from a multiphase transport model. Of particular interest are central collisions in which the averaged energy density is relatively higher than in noncentral collisions. Furthermore, influences of partonic collision on the transfer of eccentricity anisotropy

*malong@fudan.edu.cn
†glma@fudan.edu.cn
‡mayugang@fudan.edu.cn

to flow anisotropy are also investigated. This paper is organized as follows: In Sec. II, a multiphase transport (AMPT) model is briefly introduced. Results and discussion are presented in Sec. III. A summary is given in Sec. IV.

II. MODEL SETUP

The multiphase transport model (AMPT) is widely used for studying transport dynamics in relativistic heavy-ion collisions. The model consists of four main components: the initial condition, partonic interaction, hadronization (quark coalescence), and hadronic interactions [58,59]. Fluctuating initial conditions including minijet partons and soft string excitations are generated from the heavy ion jet interaction generator (HIJING) model [60]. In the string melting scenario, both excited strings and minijet partons are melted into partons, i.e., decomposed into constituent quarks according to their flavor and spin structures. The following evolution of partonic matter is described by a parton cascade model, Zhang's parton cascade (ZPC) model [61], which includes elastic partonic scatterings at present. Partons stop interacting when no parton pairs can be found within the interaction range of the perturbative QCD (pQCD) cross section. The transition from partonic matter to hadronic matter is achieved using a simple quark coalescence model which combines partons into hadrons. The final-stage hadronic interactions are modeled by a relativistic transport model (ART) including both elastic and inelastic scattering descriptions for baryon-baryon, baryon-meson, and meson-meson interactions [62].

At the parton cascade stage, the differential parton-parton elastic scattering cross section is formularized based on the leading order pQCD gluon-gluon interaction:

$$\frac{d\sigma}{dt} = \frac{9\pi\alpha_s^2}{2}\left(1+\frac{\mu^2}{s}\right)\frac{1}{(t-\mu^2)^2}, \tag{1}$$

where α_s is the strong coupling constant, s and t are the usual Mandelstam variables, and μ is the Debye screening mass in partonic matter. Previous studies show that, by setting proper parton scattering cross sections, the AMPT model with string melting scenario has been successful in describing many experimental results in heavy-ion collisions at RHIC and LHC energies [35,44,63–68].

In this study, we employ the string melting version of the AMPT model to focus on the partonic phase only. The parton cross section is set to be 3 mb according to Ref. [69], which reasonably reproduces the experimental results. Pb + Pb collision events are generated over a wide centrality range at center-of-mass energy of 5.02 TeV. Table I shows the definition of centrality classes and the corresponding mean number of participant nucleons.

TABLE I. Centrality classes of the AMPT events in Pb+Pb collisions at $\sqrt{s_{NN}} = 5.02$ TeV.

Centrality percentile	Impact parameter b (fm)	$\langle N_{\text{part}}\rangle$
0%–10%	0.0–4.9	362.8
10%–20%	4.9–7.0	263.5
20%–30%	7.0–8.6	188.2
30%–40%	8.6–10.0	131.8
40%–50%	10.0–11.2	86.1
50%–60%	11.2–12.3	53.8

III. RESULTS AND DISCUSSION

A. Parton collisions in Pb + Pb collisions

We trace the collisional history of the initially produced partons during the source evolution in Pb + Pb collisions. The total number of parton-parton scatterings suffered by each parton before its freezing out is defined as N_{coll}.

Figure 1 shows the N_{coll} distributions of the freeze-out partons for different centrality classes. As expected, partons in central Pb + Pb collisions on average suffer more partonic collisions than noncentral collisions before freezing out as the energy density is higher in more central collisions. The probability distribution shows a nonmonotonic N_{coll} dependence in central collisions which is different from that of the peripheral collisions. A peak around $N_{\text{coll}} \approx 6$ is observed for the 0–10% most central collisions. The average number of N_{coll} in 0–10% centrality is found to be roughly three times as large as that in 40–60% centrality. It indicates that the fraction of partons which never collided with other partons decreases from peripheral to central collision class.

We study in particular the spatial evolution of the initial partons in ultrarelativistic heavy-ion collisions. Figures 2 and 3 present the two-dimensional distributions of the initial partons [plots (a)–(c)] and freeze-out partons [plots (d)–(f)] in central and peripheral Pb + Pb collisions, where the initial parton distributions in the collision zone are compared with the final parton distributions for different N_{coll} intervals. We find that partons suffering small N_{coll} tend to distribute in the outer region close to the source surface whereas partons with large N_{coll} are seen concentrating more in the central area. This is consistent with the expectation that, due to the energy density distribution of the bulk matter, outgoing partons from the inner source suffer more collisions when passing through the bulk matter than partons close to the source surface.

We further investigate the partonic collision history of some selected partons before their freezing out. For a selected parton, we define those partons which collided with the selected parton during its evolution as "associated partons" of the selected parton. The numbers of parton collisions for the selected parton and associated parton are defined as $N_{\text{coll}}^{\text{sel}}$ and $N_{\text{coll}}^{\text{assoc}}$, respectively. Figures 4(a) and 4(b) show the $N_{\text{coll}}^{\text{assoc}}$ probability distributions for five $N_{\text{coll}}^{\text{sel}}$ intervals of the selected partons for peripheral and central Pb + Pb collisions, respectively. One can find that, for a selected freeze-out parton which suffered $N_{\text{coll}}^{\text{sel}}$ collisions, the number of collisions that its associated partons suffer ($N_{\text{coll}}^{\text{assoc}}$) can be distributed over a wide range. For example, for a selected parton with a small $N_{\text{coll}}^{\text{sel}}$, a long-tailed $N_{\text{coll}}^{\text{assoc}}$ distribution can be observed, suggesting that many large-$N_{\text{coll}}^{\text{assoc}}$ partons play an important role in the collisional history of the small-$N_{\text{coll}}^{\text{sel}}$ parton. We quantitatively extract the mean value of $N_{\text{coll}}^{\text{assoc}}$ for each $N_{\text{coll}}^{\text{sel}}$ interval and plot the relations as shown in Fig. 4(c). One can find that $\langle N_{\text{coll}}^{\text{assoc}}\rangle$ is larger than $\langle N_{\text{coll}}^{\text{sel}}\rangle$ at small $\langle N_{\text{coll}}^{\text{sel}}\rangle$, which indicates

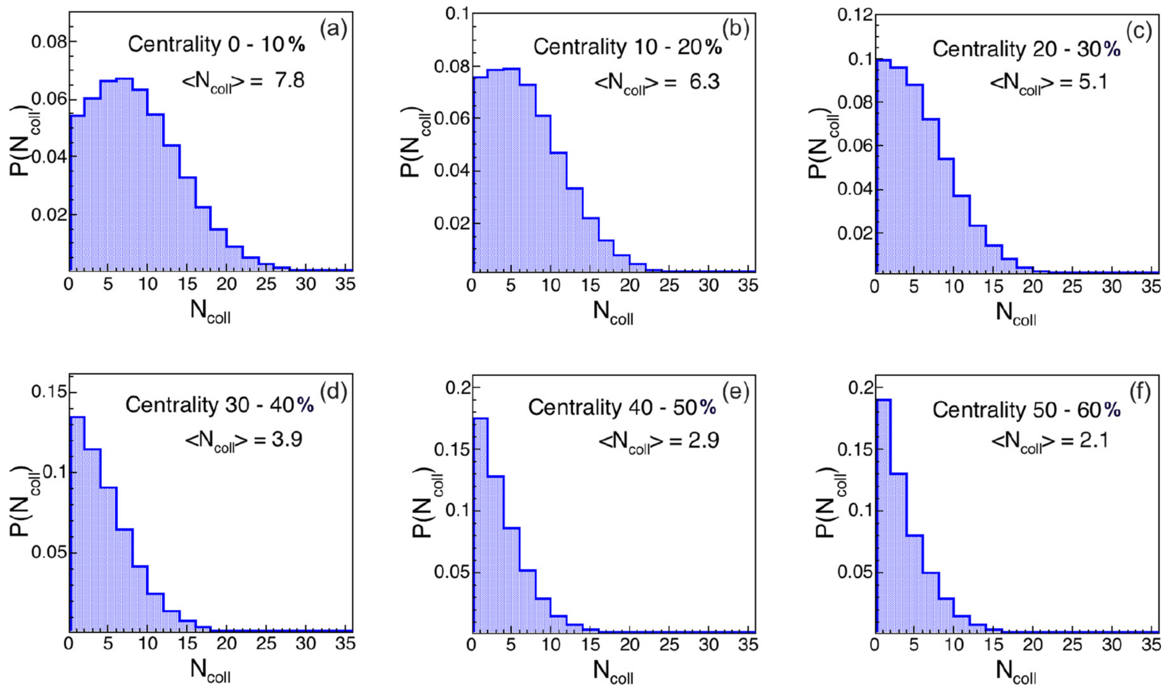

FIG. 1. Probability distributions of N_{coll} for the freeze-out partons for Pb + Pb collisions at $\sqrt{s_{NN}} = 5.02$ TeV in AMPT simulation. Results are shown for six centrality classes.

that the partons which suffer a small number of collisions prefer to collide with the partons which suffer a larger number of collisions. But with increasing $\langle N_{\text{coll}}^{\text{sel}} \rangle$, $\langle N_{\text{coll}}^{\text{assoc}} \rangle$ tends to be close to and then less than $\langle N_{\text{coll}}^{\text{sel}} \rangle$. It indicates that the partons which suffer a large number of collisions prefer to collide with the partons which suffer a small number of collisions.

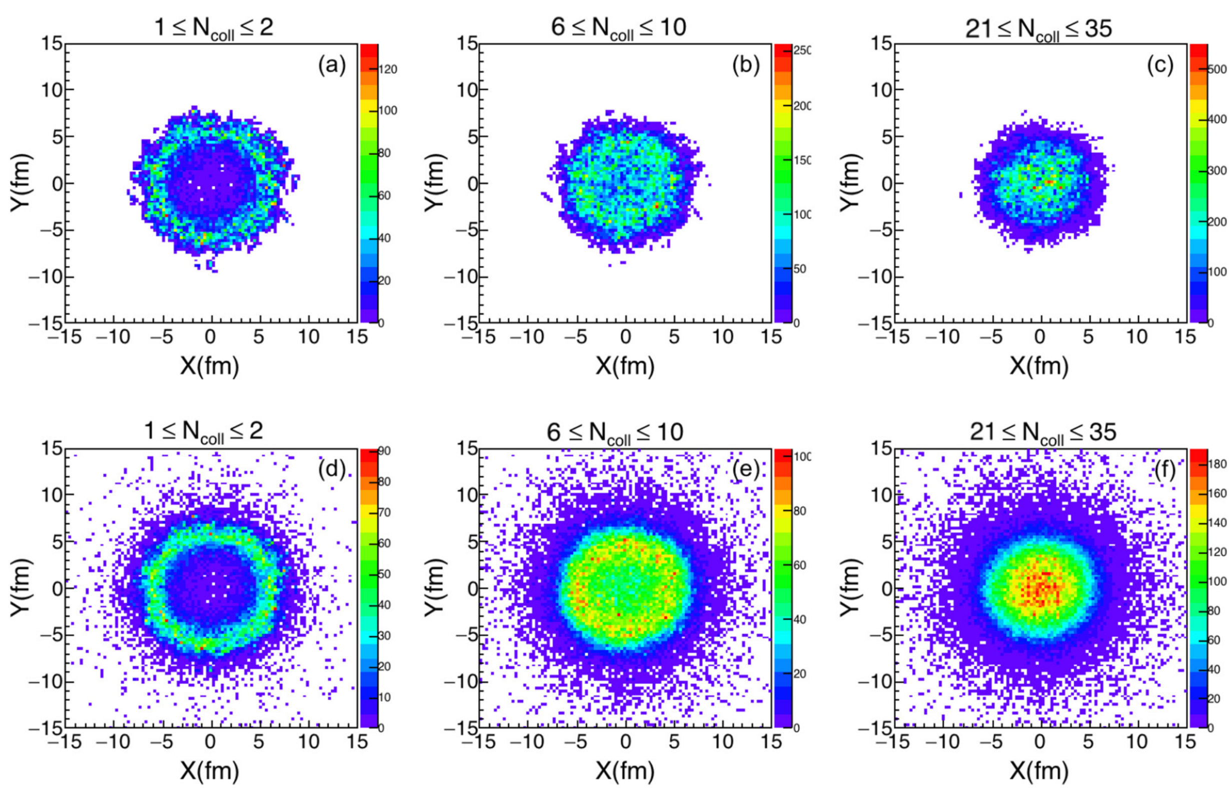

FIG. 2. Distributions of initial partons (upper panels) and freeze-out partons (lower panels) for different N_{coll} intervals in the transverse plane for the most central ($b = 0$ fm) Pb + Pb collisions at $\sqrt{s_{NN}} = 5.02$ TeV.

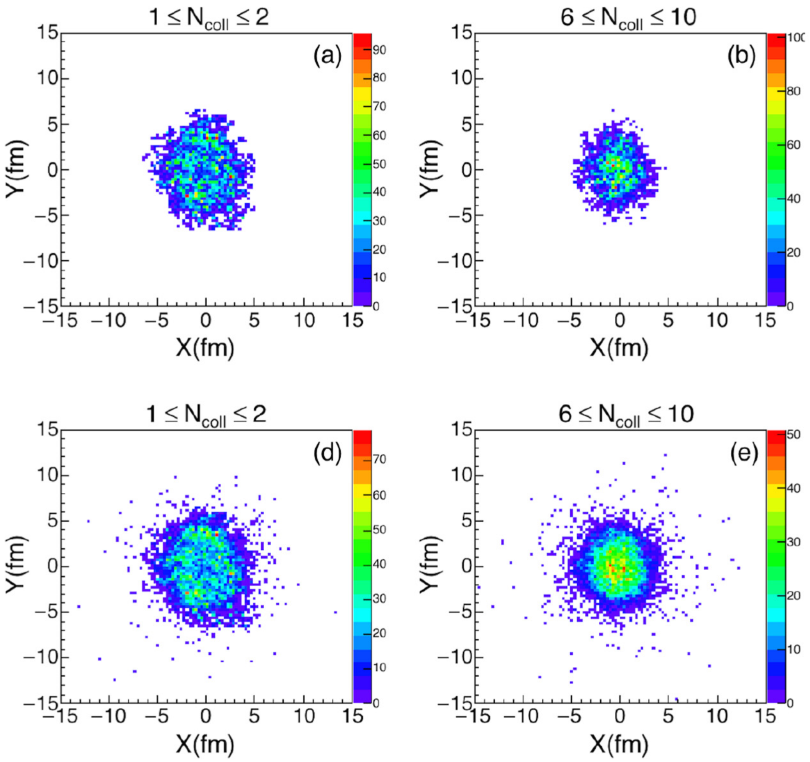

FIG. 3. Same as Fig. 2 but for $b = 11.5$ fm.

In this sense, all partons are complemented with each other during the whole evolution of the partonic phase in Pb + Pb collisions.

B. Collisional effect on the flow anisotropy

Azimuthal anisotropy coefficients v_n $(n = 2, 3, \dots)$ are typically used to characterize the different orders of harmonic flow of the collision system. In simulation studies, one can calculate v_n with respect to the participant plane of the collision event [70]. The nth-order participant plane angle ψ_n for a single event is in the form

$$\psi_n\{PP\} = \frac{1}{n}\left[\arctan\frac{\langle r^2\sin(n\varphi_{PP})\rangle}{\langle r^2\cos(n\varphi_{PP})\rangle} + \pi\right], \tag{2}$$

where r and φ_{PP} are the position and azimuthal angle of each parton in the transverse plane in the initial stage of AMPT and the bracket $\langle\cdots\rangle$ denotes per-event average. Then v_n with respect to the participant plane $\psi_n\{PP\}$ is defined as

$$v_n\{PP\} = \langle\cos[n(\phi - \psi_n\{PP\})]\rangle, \tag{3}$$

where ϕ in this study is the azimuthal angle of the parton in momentum space, and the average $\langle\cdots\rangle$ denotes event average. The above method for v_n calculation is referred to as the participant plane method. The participant plane method takes into account the initial geometric fluctuation effect, and has been widely used in many studies [50].

Besides the participant plane method, the multiparticle cumulant method was also proposed for studying flow via particle correlations. It has been successfully used in both

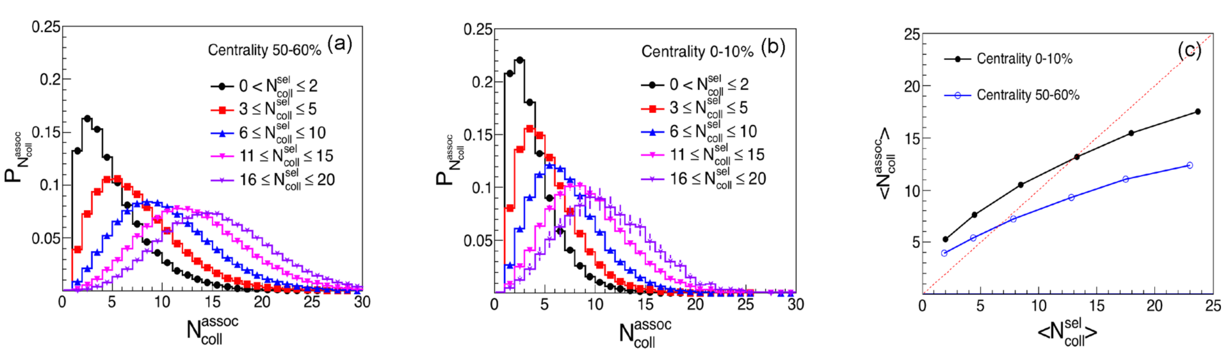

FIG. 4. The $N_{\rm coll}^{\rm assoc}$ probability distributions of the "associated parton" collided with different $N_{\rm coll}^{\rm sel}$ intervals of selected partons for two centrality classes of 50–60% (a) and 0–10% (b) in Pb + Pb collisions at $\sqrt{s_{NN}} = 5.02$ TeV. Panel (c) shows $\langle N_{\rm coll}^{\rm assoc}\rangle$ as functions of $\langle N_{\rm coll}^{\rm sel}\rangle$ for the two centrality classes.

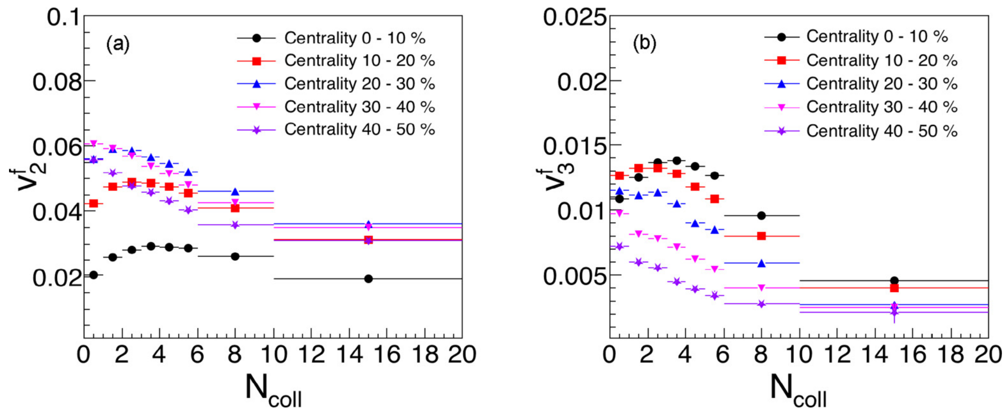

FIG. 5. v_n^f ($n = 2, 3$) of final freezeout partons from participant plane method as a function of N_{coll} for Pb + Pb collisions at $\sqrt{s_{NN}} = 5.02$ TeV in the AMPT model. Results are shown for different centrality classes.

model and experimental studies to quantified the harmonic flow [16,63,71]. Usually, the two- and four-particle cumulants can be written as

$$C_n\{2\} = \langle\langle 2\rangle\rangle, \quad C_n\{4\} = \langle\langle 4\rangle\rangle - 2\langle\langle 2\rangle\rangle^2. \tag{4}$$

The integral flow can be derived directly from two- and four-particle cumulants through the equations

$$v_n\{2\} = \sqrt{C_n\{2\}}, \quad v_n\{4\} = \sqrt[4]{-C_n\{4\}}, \tag{5}$$

and estimation of differential flow is according to

$$v_n'\{2\} = \frac{d_n\{2\}}{\sqrt{c_n\{2\}}}, \quad v_n'\{4\} = \frac{d_n\{4\}}{-c_n\{4\}^{3/4}}, \tag{6}$$

where the $d_n\{2\}$ and $d_n\{4\}$ are the two- and four-particle differential cumulants as defined in Ref. [71].

By extracting the parton information in AMPT simulation, we study the collisional effects on the development of partonic flow and eccentricity in the early stage of heavy-ion collisions.

Figure 5 shows the simulation results of the anisotropic flow of freeze-out partons as a function of N_{coll} in Pb + Pb collisions at $\sqrt{s_{NN}} = 5.02$ TeV. The second- and third-order flow harmonics of the freeze-out partons are defined as v_2^f and v_3^f respectively. Similarly to the probability distribution of N_{coll}, v_2^f shows nonmonotonic N_{coll} dependence for central collisions. A maximum value of v_2^f around $N_{\text{coll}} \approx 5$ is observed for 0–10% centrality. For peripheral collisions, v_2^f shows a similar decreasing trend and is comparably much larger in magnitude than that of central collisions. It generally shows that partons with larger N_{coll} tend to have smaller v_2^f, indicating that with increasing N_{coll} the momentum azimuthal distribution of freeze-out partons tends to be isotropic. This could be because large-N_{coll} partons come mostly from the center where the effective gradients are small. In other words, large-N_{coll} partons are less sensitive to the geometry than small-N_{coll} partons which are closer to the surface. The same conclusion also holds for v_3^f but originates basically from the initial-state fluctuations.

Besides the participant plane method, we further studied v_n^f based on multiparticle cumulant methods. Figure 6 shows the two-particle ($v_2\{2\}$) and four-particle ($v_2\{4\}$) cumulant flow results. Comparisons are made with the results from the participant plane method. It is generally found that v_2^f from cumulant methods are similar in trend with the v_2^f results from the participant plane method. An ordering of $v_2\{2\} > v_2\{\text{part}\} > v_2\{4\}$ is observed, because $v_2\{2\}$ involves flow fluctuations but $v_2\{4\}$ suppresses nonflow contributions.

Towards a more quantitative study, we compare the flow anisotropies of the initial partons (v_n^i) and final freeze-out partons (v_n^f) for $n = 2, 3$. Note that the averaged v_n for all the initial partons is zero due to the isotropy of initial azimuthal distribution in the AMPT model. As can be seen in Fig. 7, showing the change of v_n from the initial to the final stage of the partonic evolution, the parton-parton collisions generally make v_2 and v_3 increase for different N_{coll} regions. For the partons with a larger N_{coll}, the change of v_2 and v_3 is smaller, since they are more probably located at the center of the source, where more collisions may randomize their motion.

In order to quantitatively study the collisional effect on the flow harmonics, we examine the change of parton v_n after N_{coll} collisions, i.e., $\Delta v_n = v_n^f - v_n^i$. Figure 8 shows the Δv_n ($n = 2, 3$) in Pb + Pb collisions as a function of N_{coll}. Results are compared for different flow methods. Significant centrality dependence can be seen for Δv_n. It is interesting to see that in central collisions Δv_2 shows nonmonotonic N_{coll} dependence whereas Δv_3 presents monotonic N_{coll} dependence. As shown in Fig. 7, the initial intrinsic parton v_n is quite tiny; the gain in v_n is primarily due to the partonic scatterings throughout the source evolution. In general, Δv_n decreases with increasing N_{coll}, indicating that small-N_{coll} partons contribute to most of the flow anisotropies.

C. Collisional effect on the initial eccentricity

Initial geometry anisotropy of the QGP matter is a main source responsible for generating the final flow anisotropy in relativistic heavy-ion collisions. Thus, it is important to study the partonic effect on the initial spatial anisotropy. In nuclear-nuclear collisions, the spatial anisotropy of the collision zone in the transverse plane (perpendicular to the beam direction) can be characterized by the eccentricity ε_n. It has been argued that the magnitude and trend of the eccentricity imply testable predictions for final-state hadronic flow [72–75].

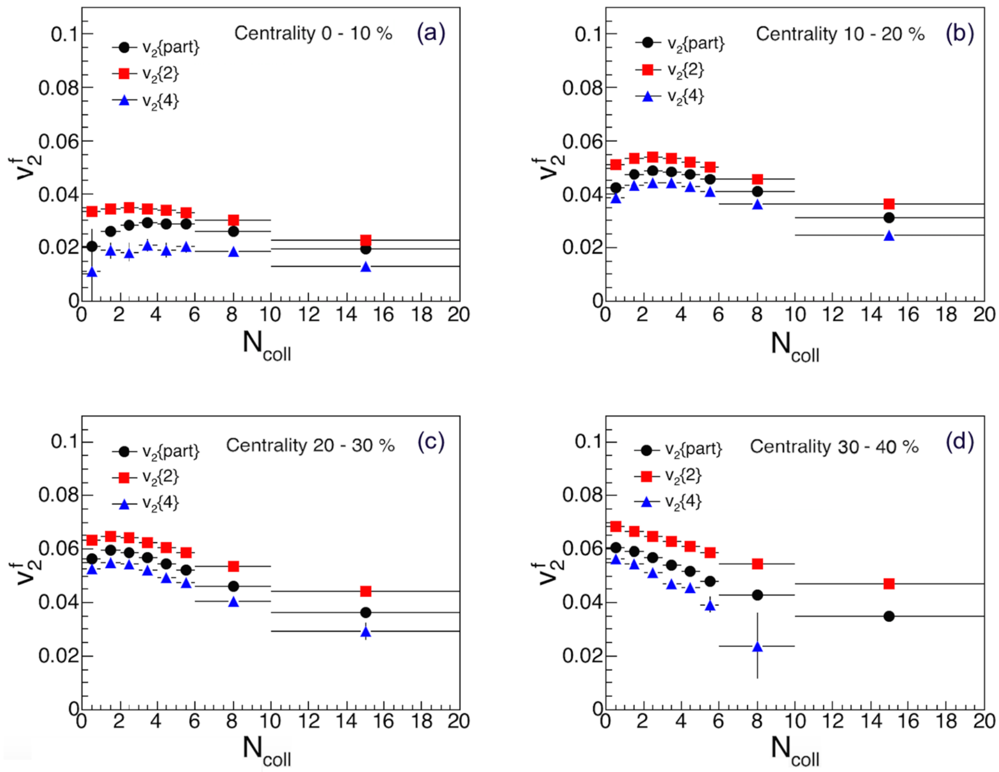

FIG. 6. v_2^f of final freeze-out partons from two-particle ($v_2\{2\}$) and four-particle ($v_2\{4\}$) cumulant methods as a function of $N_{\rm coll}$ for Pb + Pb collisions at $\sqrt{s_{NN}} = 5.02$ TeV in the AMPT model. Comparisons are made with the participant plane method for different centrality classes.

The definition of the nth-order harmonic eccentricity in the coordinate space of the participant nucleons or partons for a single collision event is in the form

$$\varepsilon_n\{\text{part}\} = \frac{\sqrt{\langle r^n \cos(n\varphi)\rangle^2 + \langle r^n \sin(n\varphi)\rangle^2}}{\langle r^n\rangle}, \tag{7}$$

where r and φ are position and azimuthal angle of each nucleon or parton in the transverse plane. $\varepsilon_n\{\text{part}\}$ characterizes the eccentricity through the distribution of participant nucleons or partons which naturally contains event-by-event fluctuation. $\varepsilon_n\{\text{part}\}$ defined in this way is usually named as "participant eccentricity."

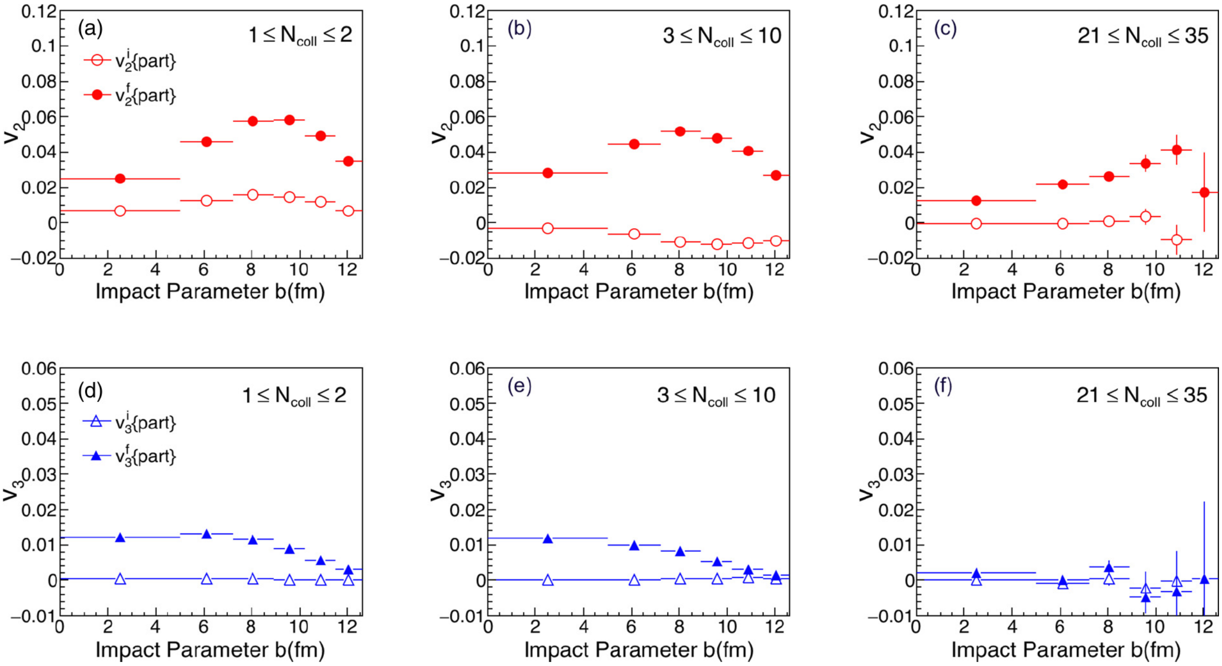

FIG. 7. v_n^i of initial state partons and v_n^f of final freeze-out partons as a function of impact parameter for different $N_{\rm coll}$ intervals.

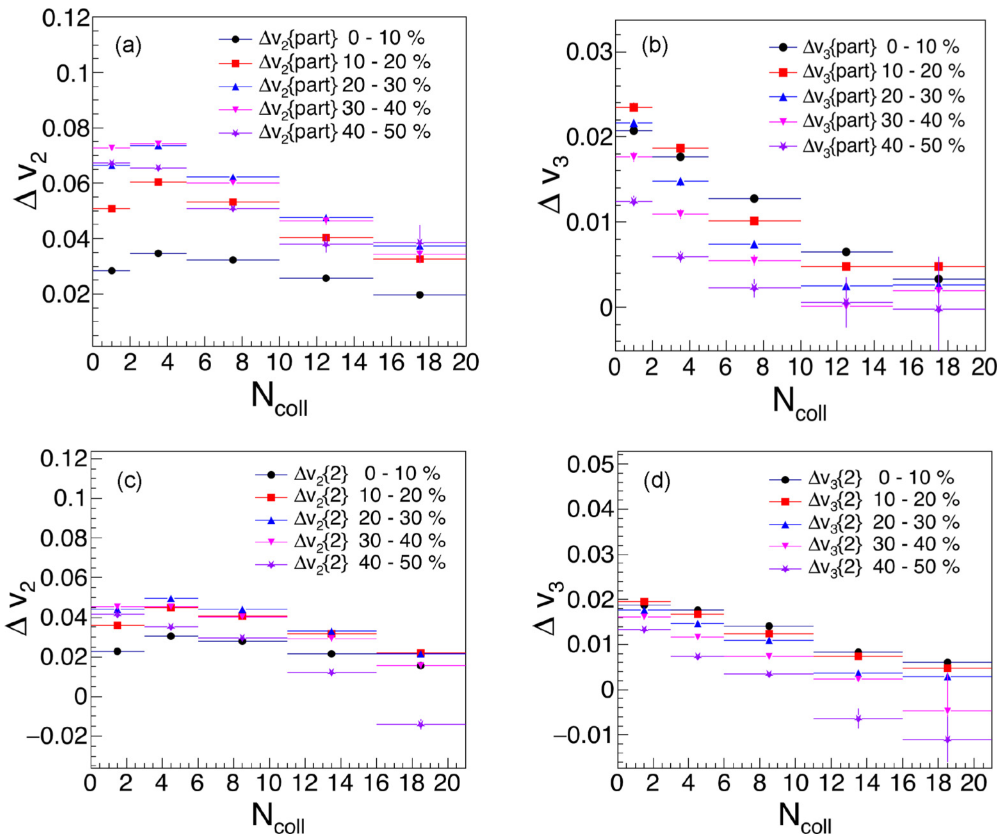

FIG. 8. The AMPT results of $\Delta v_n = v_n^f - v_n^i$ ($n = 2, 3$) as a function of N_{coll}, where the upper panels show Δv_n from the participant plane method and the lower panels show Δv_n from two-particle cumulant methods.

We study the parton collisional effects on the partonic eccentricity in Pb + Pb collisions. Figure 9 shows the AMPT results of the second- and third-order eccentricities calculated with Eq. (7). Eccentricities of the initial and final freeze-out

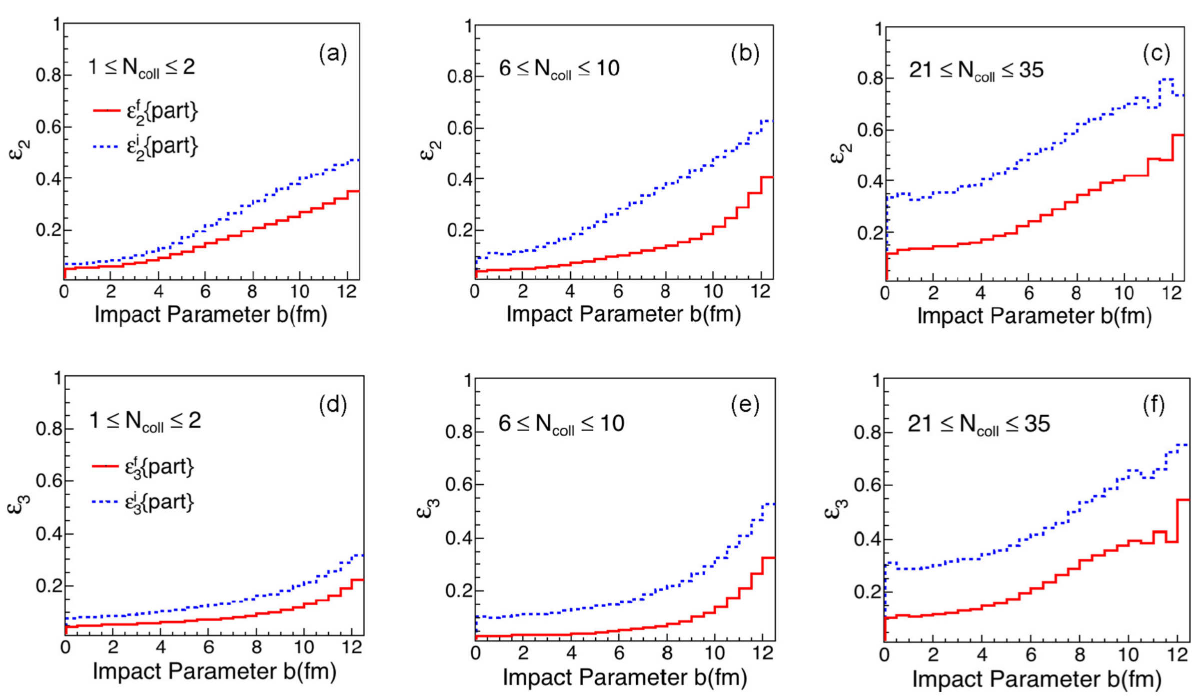

FIG. 9. $\varepsilon_2^{i,f}$\{part\} (upper panels) and $\varepsilon_3^{i,f}$\{part\} (lower panels) of the initial state and final freeze-out partons as a function of impact parameter for Pb + Pb collisions at $\sqrt{S_{NN}} = 5.02$ TeV. Simulation results are shown for different N_{coll} intervals.

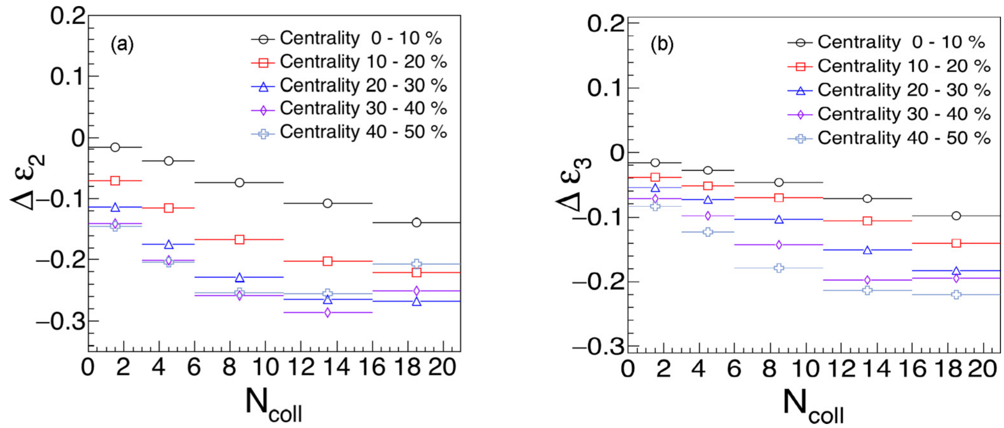

FIG. 10. The AMPT results of $\Delta\varepsilon_n = \varepsilon_n^f\{\text{part}\} - \varepsilon_n^i\{\text{part}\}$ ($n = 2, 3$) as a function of N_{coll} for different centrality classes.

partons are denoted as $\varepsilon_n^i\{\text{part}\}$ and $\varepsilon_n^f\{\text{part}\}$ respectively. Similarly to the flow harmonics, partonic scattering is found to play an important role in the evolution of eccentricities. ε_n of the freeze-out partons is larger at larger N_{coll}. One can see in the figures that parton collisions generally reduce ε_n, which is consistent with our expectation: during the expansion of the QGP source, the transition of the initial pressure gradient from coordinate space to the momentum space will significantly diminish the spatial anisotropy.

In addition, we studied $\Delta\varepsilon_n = \varepsilon_n^f\{\text{part}\} - \varepsilon_n^i\{\text{part}\}$ as a function of the number of parton collisions for different centrality classes. The results for second- and third-order harmonics are shown in Figs. 10(a) and 10(b), respectively. We find that $\Delta\varepsilon_2$ and $\Delta\varepsilon_3$ exhibit clear decreasing N_{coll} dependences. Quantitative differences are seen between the results for $\Delta\varepsilon_2$ and $\Delta\varepsilon_3$, because ε_3 is purely driven by initial fluctuations but ε_2 is driven by initial geometry.

D. Collisional effect on the flow response to the eccentricity

Impressive progress has been made in studying the final-state flow response to the initial eccentricity in relativistic heavy-ion collisions [76,77]. The success of hydrodynamical models tells us that elliptic flow v_2 and triangular flow v_3 are mainly driven by the linear response to the initial ellipticity and triangularity of the source geometry. As space-momentum correlation is also expected to be built during the partonic evolution stage; quantitative study of the partonic flow response in an event-by-event transport model is also important for understanding the development of final flow.

Based on the AMPT model simulations, we studied N_{coll} effects on the flow response by looking into the ratio $\Delta v_n/\Delta\varepsilon_n$. Since $\Delta\varepsilon_n$ ($n = 2, 3$) are negative and Δv_n ($n = 2, 3$) are positive over all the N_{coll} classes, one could take the absolute value of $\Delta v_n/\Delta\varepsilon_n$ as an estimation of the flow conversion efficiency. Figures 11 and 12 show the results for the flow conversion efficiency with respect to $\Delta\varepsilon_n$ and ε_n^i as a function of N_{coll}. Considering absolute value, results in both figures show a similar trend. The ratio of $\Delta v_n/\Delta\varepsilon_n$ presents obvious N_{coll} dependences for different centrality classes. We observe that for both elliptic and triangular flow the conversion efficiency is strongest in the collision class of 0–10%. It indicates that more collisions in more central collisions help transfer ε_n into v_n, which is a normal concept about the flow conversion efficiency, which is an integral effect of all N_{coll} partons. For the differential N_{coll} dependence, $\Delta v_n/\Delta\varepsilon_n$ ($n = 2, 3$) presents a smooth increasing trend from small to large N_{coll}, which indicates that the larger N_{coll} is, the lower the flow conversion efficiency is. The feature seems against common sense, but it can be understood through the above results that

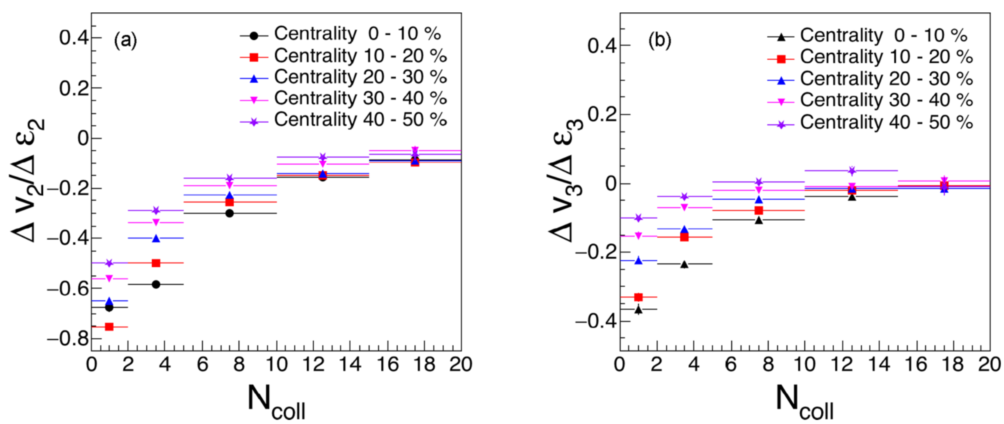

FIG. 11. Conversion efficiency $\Delta v_n/\Delta\varepsilon_n$ for $n = 2$ (left panel) and $n = 3$ (right panel) as a function of N_{coll} for Pb + Pb collisions at 5.02 TeV.

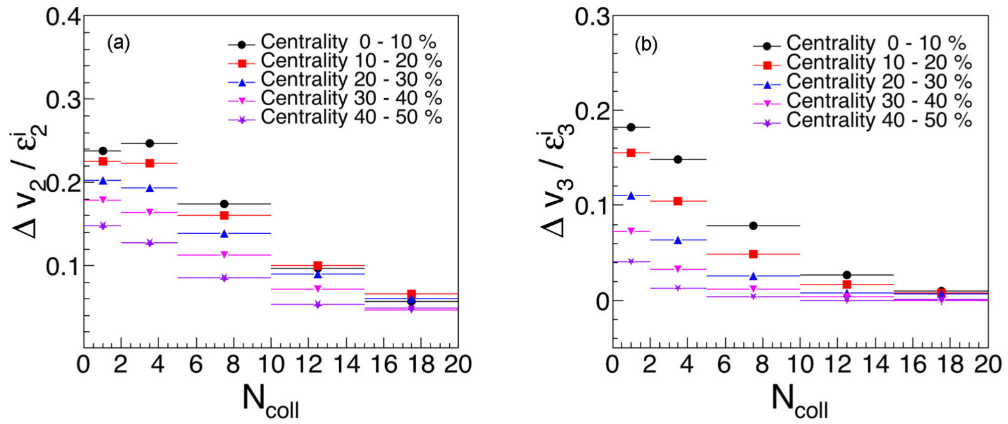

FIG. 12. $\Delta v_n/\varepsilon_n^i$ for $n = 2$ (left panel) and $n = 3$ (right panel) as a function of $N_{\rm coll}$ for Pb + Pb collisions at 5.02 TeV, where ε_n^i is the initial partonic eccentricity.

parton collisional contribution to flow change Δv_n is more significant at smaller $N_{\rm coll}$ whereas that to eccentricity change $\Delta\varepsilon_n$ is more significant at larger $N_{\rm coll}$, i.e., changes of Δv_n and $\Delta\varepsilon_n$ are not in sync with respect to $N_{\rm coll}$. But since small-$N_{\rm coll}$ and large-$N_{\rm coll}$ partons complement each other during the evolution, it is actually hard to fairly say which should be given the first credit to the generation of the final flow. In the limit of long evolution time, final eccentricity ε_n^f is supposed to approach zero, and we observe similar results for $\Delta v_n/\varepsilon_n^i$ except with the opposite sign, as shown in Fig. 12.

IV. SUMMARY

In summary, we studied initial partonic flow anisotropy (v_n) and spatial anisotropy (ε_n) in Pb + Pb collisions at center-of-mass energy of 5.02 TeV using a multiphase transport model. By tracing the partonic cascade history in AMPT, the effect of the parton-parton collisions was intensively investigated. We find that partonic collision plays an important role in the development of flow anisotropies in heavy-ion collisions. We find that the partons which suffer a small number of collisions prefer to collide with the partons which suffer a larger number of collisions, and vice versa. The change of v_n decreases with increasing $N_{\rm coll}$, indicating that small-$N_{\rm coll}$ partons contribute to most of the flow anisotropies. However, the change of eccentricity is more significant for the large-$N_{\rm coll}$ partons. As a result, the partons with larger $N_{\rm coll}$ show a lower flow conversion efficiency, which reflect the differential behaviors of the flow conversion efficiency with respect to $N_{\rm coll}$. However, since small-$N_{\rm coll}$ and large-$N_{\rm coll}$ partons always complement each other, it is hard to rank their roles in generating flow.

However, one has to be aware that although the AMPT model provides an effective tool to simulate and study parton-parton collisions in relativistic heavy-ion collisions, the initial partonic source configured using constituent quarks in the string-melting scenario could introduce some intrinsic bias into our study, since the created QGP should consist of both current quarks and gluons. In addition, the approximation of the model treatment of the parton interactions is in a way analogous to gluon-gluon elastic interaction based on the leading order pQCD cross section, which could also introduce some bias and lead to an incomplete or improper description, since the QGP evolution involves nonperturbative QCD processes. Nevertheless, such a simplified picture of the partonic evolution in this model is expected to provide some guides to the study of the effect on the conversion rules of the initial eccentricity to the final flow anisotropy.

As anisotropic flow of initial partons will transfer to the final hadrons which are formed from the coalescence of freeze-out quarks in the transport model, further study by tracing the hadronization and hadronic evolution of particles would be important for fully understanding the complete behavior of the anisotropic flow. We postpone such investigations for our future study.

ACKNOWLEDGMENTS

We thank A. Bzdak and Z.-W. Lin for helpful discussions. This work is supported in part by the National Natural Science Foundation of China under Contracts No. 11961131011, No. 11890710, No. 11890714, No. 11835002, No. 11421505, No. 11905034, the Key Research Program of Frontier Sciences of Chinese Academy of Sciences under Grant No. QYZDJ-SSW-SLH002, the Strategic Priority Research Program of Chinese Academy of Sciences under Grant No. XDB34030000, and the Guangdong Major Project of Basic and Applied Basic Research No. 2020B0301030008.

[1] J.-Y. Ollitrault, Phys. Rev. D **46**, 229 (1992).

[2] S. A. Voloshin, A. M. Poskanzer, and R. Snellings, in *Relativistic Heavy Ion Physics*, Landolt-Börnstein - Group I Elementary Particles, Nuclei and Atoms, Vol. 23, edited by R. Stock (Springer-Verlag, Berlin, Heidelberg, 2010), pp. 293–333.

[3] K. H. Ackermann *et al.* (STAR Collaboration), Phys. Rev. Lett. **86**, 402 (2001).

[4] D. Teaney, J. Lauret, and E. V. Shuryak, Phys. Rev. Lett. **86**, 4783 (2001).

[5] P. Romatschke and U. Romatschke, Phys. Rev. Lett. **99**, 172301 (2007).

[6] X. F. Luo and N. Xu, Nucl. Sci. Tech. **28**, 112 (2017).
[7] J. Chen, D. Keane, Y.-G. Ma, A. Tang, and Z. Xu, Phys. Rep. **760**, 1 (2018).
[8] J. Adams, C. Adler *et al.* (STAR Collaboration), Phys. Rev. Lett. **92**, 062301 (2004).
[9] L. Adamczyk *et al.* (STAR Collaboration), Phys. Rev. C **88**, 014904 (2013).
[10] A. Adare *et al.* (PHENIX Collaboration), Phys. Rev. Lett. **107**, 252301 (2011).
[11] J. Margutti *et al.* (ALICE Collaboration), Nucl. Phys. A **982**, 367 (2019).
[12] S. Acharya *et al.* (ALICE Collaboration), Phys. Rev. Lett. **123**, 142301 (2019).
[13] B. Abelev *et al.* (ALICE Collaboration), Phys. Lett. B **719**, 18 (2013).
[14] G. Aad *et al.*, Phys. Rev. Lett. **110**, 182302 (2013).
[15] S. Chatrchyan *et al.*, Phys. Lett. B **718**, 795 (2013).
[16] B. B. Abelev *et al.* (ALICE Collaboration), Phys. Rev. C **90**, 054901 (2014).
[17] A. Adare *et al.* (PHENIX Collaboration), Phys. Rev. Lett. **115**, 142301 (2015).
[18] C. Aidala *et al.* (PHENIX Collaboration), Phys. Rev. C **95**, 034910 (2017).
[19] V. Khachatryan *et al.*, Phys. Rev. Lett. **115**, 012301 (2015).
[20] C. Aidala *et al.* (PHENIX Collaboration), Phys. Rev. Lett. **120**, 062302 (2018).
[21] J. Adam *et al.* (STAR Collaboration), Phys. Rev. Lett. **122**, 172301 (2019).
[22] U. Heinz and R. Snellings, Annu. Rev. Nucl. Part. Sci. **63**, 123 (2013).
[23] U. Heinz, J. Phys. G: Nucl. Part. Phys. **31**, S717 (2005).
[24] C. Gale, S. Jeon, and B. Schenke, Int. J. Mod. Phys. **A28**, 1340011 (2013).
[25] Z. Qiu and U. Heinz, AIP Conf. Proc. **1441**, 774 (2012).
[26] H. Song, S. A. Bass, U. Heinz, T. Hirano, and C. Shen, Phys. Rev. Lett. **106**, 192301 (2011).
[27] H. Song, Y. Zhou, and K. Gajdosova, Nucl. Sci. Tech. **28**, 7 (2017).
[28] B. Schenke, S. Jeon, and C. Gale, Phys. Rev. Lett. **106**, 042301 (2011).
[29] B. H. Alver, C. Gombeaud, M. Luzum, and J.-Y. Ollitrault, Phys. Rev. C **82**, 034913 (2010).
[30] L.-W. Chen, C. M. Ko, and Z.-W. Lin, Phys. Rev. C **69**, 031901(R) (2004).
[31] A. Bzdak and G.-L. Ma, Phys. Lett. B **781**, 117 (2018).
[32] M.-W. Nie, P. Huo, J. Jia, and G.-L. Ma, Phys. Rev. C **98**, 034903 (2018).
[33] A. Bzdak and G.-L. Ma, Phys. Rev. Lett. **113**, 252301 (2014).
[34] J. L. Nagle and W. A. Zajc, Annu. Rev. Nucl. Part. Sci. **68**, 211 (2018).
[35] L. X. Han, G. L. Ma, Y. G. Ma, X. Z. Cai, J. H. Chen, S. Zhang, and C. Zhong, Phys. Rev. C **84**, 064907 (2011).
[36] J. D. Orjuela Koop, A. Adare, D. McGlinchey, and J. L. Nagle, Phys. Rev. C **92**, 054903 (2015).
[37] S. Huang, Z. Chen, W. Li, and J. Jia, Phys. Rev. C **101**, 021901(R) (2020).
[38] L. He, T. Edmonds, Z.-W. Lin, F. Liu, D. Molnar, and F. Wang, Phys. Lett. B **753**, 506 (2016).
[39] Z.-W. Lin, L. He, T. Edmonds, F. Liu, D. Molnar, and F. Wang, Nucl. Phys. A **956**, 316 (2016).
[40] M. Djordjevic, Phys. Rev. C **74**, 064907 (2006).
[41] A. Adil, M. Gyulassy, W. Horowitz, and S. Wicks, Phys. Rev. C **75**, 044906 (2007).
[42] G.-Y. Qin, J. Ruppert, C. Gale, S. Jeon, G. D. Moore, and M. G. Mustafa, Phys. Rev. Lett. **100**, 072301 (2008).
[43] G. R. Shin, S. A. Bass, and B. Müller, J. Phys. G: Nucl. Part. Phys. **37**, 105112 (2010).
[44] L. Ma, G. L. Ma, and Y. G. Ma, Phys. Rev. C **89**, 044907 (2014).
[45] G.-L. Ma and A. Bzdak, Nucl. Phys. A **956**, 745 (2016).
[46] T. Edmonds, Q. Li, and F. Wang, Nucl. Phys. A **966**, 124 (2017).
[47] Z. Qiu and U. W. Heinz, Phys. Rev. C **84**, 024911 (2011).
[48] R. A. Lacey, A. Taranenko, J. Jia, D. Reynolds, N. N. Ajitanand, J. M. Alexander, Y. Gu, and A. Mwai, Phys. Rev. Lett. **112**, 082302 (2014).
[49] B. Alver and G. Roland, Phys. Rev. C **81**, 054905 (2010).
[50] R. D. de Souza, J. Takahashi, T. Kodama, and P. Sorensen, Phys. Rev. C **85**, 054909 (2012).
[51] B. Alver *et al.* (STAR Collaboration), Phys. Rev. Lett. **104**, 142301 (2010).
[52] P. Sorensen, J. Phys. G: Nucl. Part. Phys. **34**, S897 (2007).
[53] R. Andrade, F. Grassi, Y. Hama, T. Kodama, and O. Socolowski, Phys. Rev. Lett. **97**, 202302 (2006).
[54] H. Petersen, G.-Y. Qin, S. A. Bass, and B. Müller, Phys. Rev. C **82**, 041901(R) (2010).
[55] G.-L. Ma and X.-N. Wang, Phys. Rev. Lett. **106**, 162301 (2011).
[56] L. Ma, G. L. Ma, and Y. G. Ma, Phys. Rev. C **94**, 044915 (2016).
[57] J. Wang, Y. G. Ma, G. Q. Zhang, D. Q. Fang, L. X. Han, and W. Q. Shen, Nucl. Sci. Tech. **24**, 030501 (2013).
[58] B. Zhang, C. M. Ko, B.-A. Li, and Z. Lin, Phys. Rev. C **61**, 067901 (2000).
[59] Z.-W. Lin, C. M. Ko, B.-A. Li, B. Zhang, and S. Pal, Phys. Rev. C **72**, 064901 (2005).
[60] X.-N. Wang and M. Gyulassy, Phys. Rev. D **44**, 3501 (1991).
[61] B. Zhang, Comput. Phys. Commun. **109**, 193 (1998).
[62] B.-A. Li and C. M. Ko, Phys. Rev. C **52**, 2037 (1995).
[63] Y. Zhou, K. Xiao, Z. Feng, F. Liu, and R. Snellings, Phys. Rev. C **93**, 034909 (2016).
[64] M. W. Nie and G. L. Ma, Nucl. Sci. Tech. **37**, 100519 (2014).
[65] Y. F. Xu, Y. J. Ye, J. H. Chen, Y. G. Ma, S. Zhang, and C. Zhong, Nucl. Sci. Tech. **27**, 87 (2016).
[66] H. Wang, J. H. Chen, Y. G. Ma *et al.*, Nucl. Sci. Tech. **30**, 185 (2019).
[67] X. H. Jin, J. H. Chen, Y. G. Ma, S. Zhang, C. J. Zhang, and C. Zhong, Nucl. Sci. Tech. **29**, 54 (2018).
[68] Z. W. Xu, S. Zhang, Y. G. Ma, J. H. Chen, and C. Zhong, Nucl. Sci. Tech. **29**, 186 (2018).
[69] Z.-W. Lin, Phys. Rev. C **90**, 014904 (2014).
[70] S. A. Voloshin, A. M. Poskanzer, A. Tang, and G. Wang, Phys. Lett. B **659**, 537 (2008).
[71] A. Bilandzic, R. Snellings, and S. Voloshin, Phys. Rev. C **83**, 044913 (2011).
[72] M. Miller and R. Snellings, arXiv:nucl-ex/0312008.
[73] R. A. Lacey, R. Wei, J. Jia, N. N. Ajitanand, J. M. Alexander, and A. Taranenko, Phys. Rev. C **83**, 044902 (2011).
[74] H.-J. Drescher and Y. Nara, Phys. Rev. C **76**, 041903(R) (2007).
[75] W. Broniowski, P. Bożek, and M. Rybczyński, Phys. Rev. C **76**, 054905 (2007).
[76] H. Petersen, R. La Placa, and S. A. Bass, J. Phys. G **39**, 055102 (2012).
[77] H. Niemi, G. S. Denicol, H. Holopainen, and P. Huovinen, Phys. Rev. C **87**, 054901 (2013).